Knowledge-Based Classification of Polarimetric SAR Images

Leland E. Pierce, Fawwaz T. Ulaby, Kamal Sarabandi, and M. Craig Dobson

Abstract—**In preparation for the flight of the Shuttle Imaging Radar-C (SIR-C) on board the Space Shuttle in the spring of 1994, a Level-1 automatic classifier was developed on the basis of polarimetric SAR images acquired by the JPL AirSAR system. The classifier uses L- and C-Band polarimetric SAR measurements of the imaged scene to classify individual pixels into one of four categories: tall vegetation (trees), short vegetation, urban, or bare surface, with the last category encompassing water surfaces, bare soil surfaces, and concrete or asphalt-covered surfaces. The classifier design uses knowledge of the nature of radar backscattering from surfaces and volumes to construct appropriate discriminators in a sequential format. The classifier, which was developed using training areas in a test site in Northern Michigan, was tested against independent test areas in the same test site and in another site imaged three months earlier. Among all cases and all categories, the classification accuracy ranged between 91% and 100%.**

I. Introduction

SYNTHETIC aperture radar (SAR) is capable of generating high-resolution images of terrain, and, when operated in a polarimetric mode, it records the scattering matrix of each pixel in the imaged scene [1]. To reduce the effects of speckle, which is characteristic of fully focused SAR images, multiple pixels are averaged together prior to using the image for the extraction of quantitative information. The images used in the present study were generated by the JPL AirSAR system, which operated at P-, L-, and C-Bands [2]. Each image consisted of 1024 × 750 pixels, each representing nominally an area 12 m in azimuth × 6.6 m in slant range, or 12 m × 10 m average on the ground surface (Table I), with each such pixel being an average of four looks (or, equivalently, four fully focused pixels). The incidence angle ranged from approximately 30° at the near range (top) of the image to 60° at the far range (bottom).

The motivation of the present study is to develop a Level-1 classifier capable of accurately classifying the pixels in the imaged scene into four terrain categories (classes): tall vegetation (trees), short vegetation, urban, and bare surfaces (which includes water surfaces, bare soil surfaces, and road surfaces). In an earlier SAR classifier [3] all vegetation was lumped into one class: insufficient for our future needs.

Manuscript received October 29, 1993; revised March 14, 1994.

The authors are with the Radiation Laboratory, Department of Electrical Engineering and Computer Science, University of Michigan, Ann Arbor, MI 48109.

IEEE Log Number 9403652.

TABLE I
SAR Image Attributes

JPL AirSAR Test Sites	L-Band: 1.25 GHz, C-Band: 5.3 GHz Pellston, MI; Raco, MI
Pixel spacing Image sizes	12 m azimuth, x × 6.6 m slant range, y 1024 pixels az. × 750 pixels range 12.4 Km az. × 7.5 Km range Each is nominally a 4-look pixel

Simulated annealing was used by Rignot and Chellappa in an attempt to post-process the results of an MLE classifier [4] and performed quite well, yielding better than 95% classification accuracy for up to 13 classes. However, simulated annealing is a complex and time-consuming procedure to apply over an entire image. Wong and Posner [5] developed a clustering technique that can automatically devise the best number of classes and their means in feature space using a simulated annealing procedure. The classifier was based on the Mahalonobis distance [6] from each of these class means. While classification accuracies were not given, the procedure performed quite well, visually.

Another classifier, similar in methodology to the present work was presented by Moghaddam and Freeman [7]. A set of hierarchical decision rules was used to distinguish between basic land cover types. No published accuracies were given, and our own experience with their code has been disappointing.

The classifier developed here is to use only L- and C-Band data as input because the classifier is part of a broader program at the University of Michigan aimed at the development of an automatic information extraction processor that can be applied to the image data expected from the Shuttle Imaging Radar-C/X-SAR system, that is scheduled for flight on the Space Shuttle in April 1994. The SIR-C/X-SAR system has been designed to produce polarimetric radar images at L- and C-bands, and VV-polarized images at X-Band.

Fig. 1 depicts the eventual structure of the information processor. Following full calibration of the SAR images, a Level-1 classifier is used to classify the scene into the four aforementioned classes. For the bare surfaces, contextual information is to be used when separating water surfaces from bare ground surfaces. For the latter, an inversion algorithm [8] is applied to determine the soil moisture content and surface roughness. In practice, bare

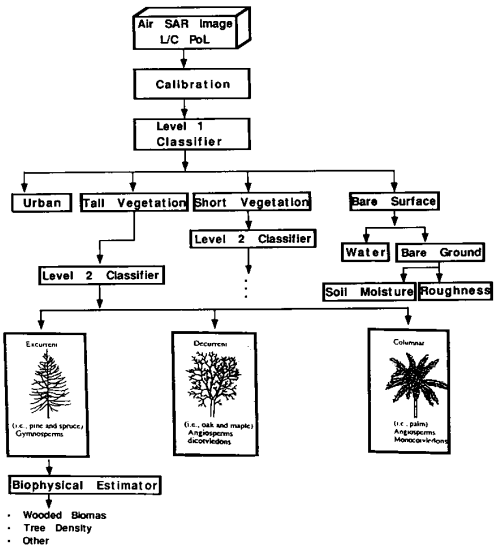

Fig. 1. Eventual structure of the SAR image information processor.

soil surfaces include surfaces with very short vegetation cover (less than 15 cm in height).

For the short vegetation and tall vegetation classes, Level-2 classifiers are to be applied for further discrimination on the basis of the structure of the vegetation. For trees, for example, the Level-2 classifier is intended to classify trees as excurrent, decurrent, or columnar. For each type of tree, a biophysical estimator, possibly in the form of a trained neural network, is to be used to estimate some of the biophysical parameters of the forest canopy, such as woody biomass and tree density. The Level-2 classifiers and biophysical estimators are in the final states of development and will be the subject of future papers. The present paper focuses on the design and operation of the Level-1 classifier.

II. Image Attributes

As mentioned earlier, the classifier uses polarimetric L- and C-Band images. Each pixel is characterized by four measured quantities at L-Band: $\sigma^0_{vv}(L)$, $\sigma^0_{hh}(L)$, $\sigma^0_{hv}(L)$, and $\zeta(L)$, and a similar set at C-Band where σ^0_{vv}, σ^0_{hh}, and σ^0_{hv} are the backscattering coefficients and ζ is the co-polarized phase difference $(\phi_{hh} - \phi_{vv})$ [9]. Although the cross-polarized phase difference $(\phi_{hv} - \phi_{vv})$ is also available from the measured polarimetric response, it contains no useful information about the target because it is uniformly distributed over $[0, 2\pi]$ for most distributed targets [10].

In addition to these eight image attributes, the classifier uses textural information by computing the normalized variance for each pixel. Using a 5×5 pixel window centered at the pixel of interest, the mean, μ, and standard deviation, σ, of the 25 pixels is computed for each magnitude (VV, HH, and HV). The measured normalized variance $(\sigma/\mu)^2$, for a given polarization, is comprised of two components: a component due to specke, $(\sigma/\mu)^2_s$, and a component due to scene texture (spatial inhomogeneity) at the SAR resolution scale [11]. The latter is denoted $(\sigma/\mu)^2_t$. The measured normalized variance is related to the individual variances through [11]:

$$(\sigma/\mu)^2 = (\sigma/\mu)^2_s + (\sigma/\mu)^2_t + (\sigma/\mu)^2_s(\sigma/\mu)^2_t. \quad (1)$$

Denoting $M = (\sigma/\mu)^2$ as the measured variance, $S = (\sigma/\mu)^2_s$ as the speckle variance, and $T = (\sigma/\mu)^2_t$ as the texture variance, (1) can be rewritten as

$$M = S + T + ST. \quad (2)$$

The speckle variance S is target-independent and is a function of the number of independent samples, N, contained in the processed measurements represented by each image pixel:

$$S = (\sigma/\mu)^2_s = 1/N \quad (3)$$

The value of N can be determined from knowledge of the multilook processing algorithm, or it can be estimated directly from the image by calculating the variance for a textureless target ($T = 0$), such as a calm water surface. In the present study, a portion of one of the lakes in the imaged scene was used for that purpose, which provided the result $S = 0.195$, or equivalently $N = 5$. It should be noted that the speckle variance is the same for all polarizations. With S known and M calculated from the 5×5 pixel window, (2) was then used to compute the image texture, T, for each pixel:

$$T = \frac{M - S}{1 + S}. \quad (4)$$

Thus, in addition to the original eight image attributes, texture provides an additional set of six attributes, (three polarizations $\times$ two bands). For notational purposes, the texture for VV polarization at L-Band is denoted $T_{vv}(L)$, and similarly for other frequency-polarization combinations.

The first part of the study was conducted using L- and C-Band AirSAR images of a test site located in northern Michigan, which will henceforth be referred to as the Pellston site. This test site consists of a variety of conifer and deciduous trees, while the main agricultural crops are grass-like (alfalfa, barley). There are also small urban areas, as well as lakes. This provides sufficient variety to train and test the classifier. Extensive ground truth measurements have been conducted for biomass inversion studies here. This effort has resulted in a good familiarity with the area, which is very important during classification for choice of training and test stands, as well as for understanding its performance in other areas.

Specifically, Fig. 2 shows a color-composite L-Band SAR image of the area from July 10, 1990. Training and test stands are clearly marked. There is only one urban region (Pellston), so no test/training division was possible. The tall vegetation category was trained with both aspens and pines at low and high incidence angles, then

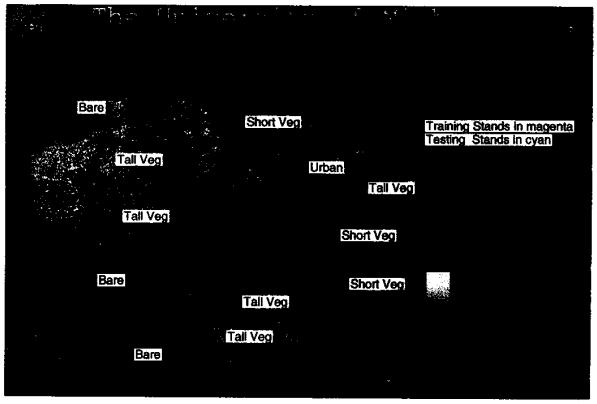

Fig. 2. Pellston test site showing training and test stands used during classification.

tested with other stands of the same type but different incidence angles. The short vegetation class was based solely on grasslands, cultivated and fallow (airport). Water was the only large bare feature in this image, and so the bare class was trained and tested with water alone. However, an apron and the runways at the airport were successfully classified as bare.

III. Classifier Design

The input data space consists of 14 channels, corresponding to the image attributes described in the previous section. All of these channels, however, are partially correlated with one another. Our initial attempt at developing a classifier was based on the application of traditional pattern recognition techniques such as the Bayesian estimator and the principal components approach [12], [13]. Although mathematically rigorous, these techniques did not lead to classifiers with good classification accuracy. As an alternative, we pursued a different approach that relied very heavily on our understanding of the physics of the scattering process and the experience gained from extensive experimental measurements and theoretical analyses conducted for various types of terrain media. We call the result of this approach a "knowledge-based classifier."

Fig. 3 provides an outline of the classifier design procedure. The first step attempts to separate "urban" pixels from everything else where an urban pixel refers to a ground area containing man-made physical structures such as buildings. Scattering by such structures is characterized by a double-bounce reflection mechanism resulting in a co-polarized phase difference ζ close to $\pm 180°$. Additionally, urban scenes exhibit higher values of image texture than do other distributed targets. Fig. 4(a) shows the boundaries of the urban/nonurban discriminator based on ζ_L and $T_{hh}(C)$. Urban pixels are classified as urban with an accuracy of 100%, while a few percent of the nonurban pixels are incorrectly classified as urban. This was purposely done to make sure that all the urban pixels were correctly classified to ensure that urban features were not incorrectly identified as trees. The majority of the

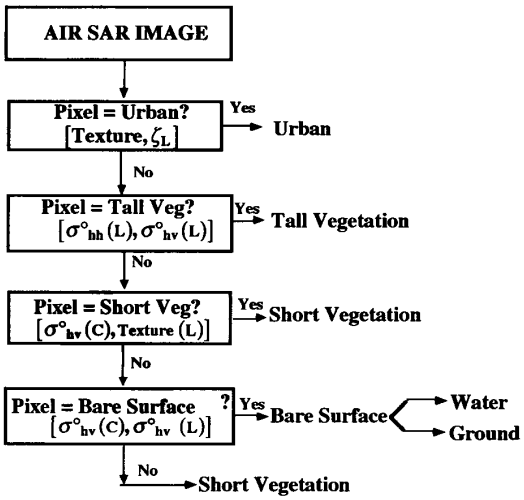

Fig. 3. Classifier design.

misclassified pixels are in areas close to the city of Pellston and along roads and highways (Fig. 5), suggesting that in reality these are "mixed" pixels including buildings along roads and lakefronts.

After removing all pixels classified as urban from further consideration, the next step is to identify those that are tall vegetation. The single most useful channel in this regard is $\sigma^0_{hv}(L)$, the cross-polarized L-Band backscattering coefficient. This is evident in Fig. 4(b) which shows that tall vegetation can be easily discriminated against the other two remaining categories (bare surface and short vegetation) using this channel. Physically, this is due to large branches in the crown, which generate a much larger cross-polarized return that do smaller leaves and grass. The discrimination can be improved slightly with the additional use of $\sigma^0_{hh}(L)$ (the final classification results are summarized later in Section IV).

After removal of the tall vegetation pixels from further consideration, classifying the remaining pixels among the last two classes (bare surface and short vegetation) involves a two-step process. In the first step, short vegetation pixels are identified on the basis of $\sigma^0_{hv}(C)$ and $T^0_{vv}(L)$, as seen in Fig. 4(c). The remaining pixels are classified as bare if both cross-polarized returns are very low [Fig. 4(d)], while the remaining pixels with a higher cross-polarized return are classified as short vegetation. Physically, water and other bare surfaces are expected to give very low cross-polarized returns due to a lack of large angled features. Very rough water, however, has an increased cross-polarized return, but also increased texture, especially in $\sigma^0_{vv}(L)$.

Pixels that are not classified initially as short vegetation, nor later as bare, are reclassified as short vegetation. This final assignment rule was used because most of the "unclaimed" pixels did indeed belong to the short-vegetation class.

In order for other investigators to try out this classifier on their own images, the equations used for each rule are

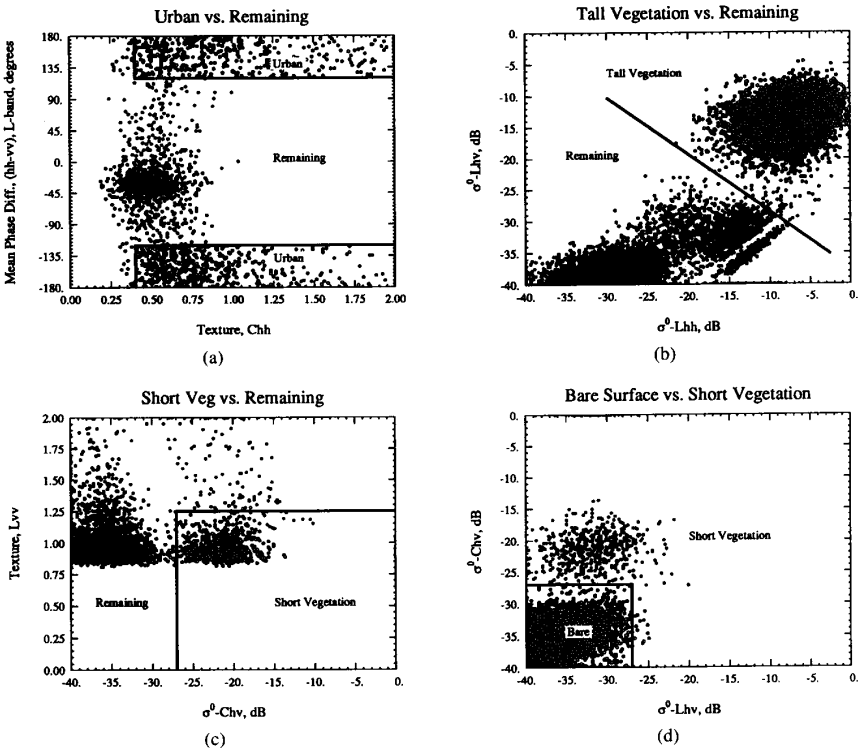

Fig. 4. Decision Rules: (a) Urban versus remaining. (b) Tall Vegetation versus remaining. (c) Short Vegetation versus remaining. (d) Bare Surface versus Short vegetation.

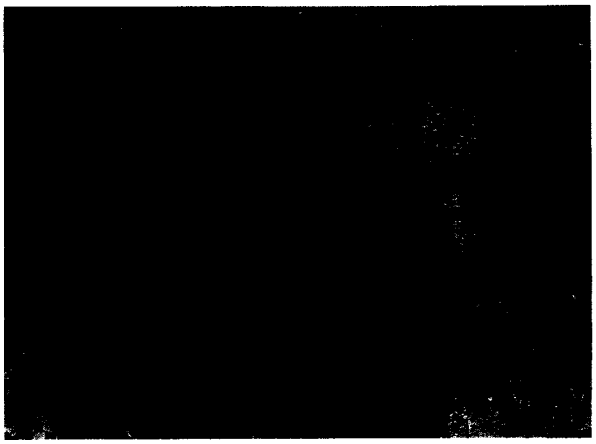

Fig. 5. Fully classified Pellston test site. Urban is in white, tall vegetation is green, short vegetation is light brown, bare is blue.

given here. The first rule, to classify urban, uses textures and a phase difference [see Fig. 4(a) for a graphical representation of half of this rule]. If the following conditions are all true, then the pixel is classified as urban:

$$T_{hh}(L) > 0.5, \qquad T_{vv}(L) > 0.95,$$
$$T_{hh}(C) > 0.4 \quad \text{and} \quad |\zeta(L)| > 120°. \qquad (5)$$

The second rule to classify tall vegetation, uses L-Band powers and draws a line to separate the two clusters [see Fig. 4(b)]. If the following condition is true, then the pixel is classified as tall vegetation:

$$\sigma^0_{hv}(L) > -0.91[\sigma^0_{hh}(L) + 5 \text{ dB}] - 33 \text{ dB} \qquad (6)$$

where σ^0 is expressed in dB. The third rule, to classify short vegetation, uses C-Band power and L-Band texture [see Fig. 4(c)]. If the following conditions are true, then the pixel is classified as short vegetation:

$$\sigma^0_{hv}(C) > -27 \text{ dB}, \quad \text{and} \quad T_{vv}(L) < 1.25. \qquad (7)$$

The fourth rule, to classify bare surfaces and short vegetation, uses cross-polarized L- and C-Band powers [see Fig. 4(d)]. If the following conditions are true, then the pixel is classified as a bare surface, while if false it is classified as short vegetation:

$$\sigma^0_{hv}(C) \leq -27 \text{ dB}, \quad \text{and} \quad \sigma^0_{hv}(L) < -27 \text{ dB}. \qquad (8)$$

Fig. 5 shows the first step of the classification. As seen in Fig. 5, there are many pixels that were classified as urban in areas where houses are expected: the city itself, major roads, and the lakefront. However, there are also a few in unexpected places, like in the middle of a forest. These pixels are very likely due to a large double-bounce from the edge of a small clearing in the forest. This would

explain both large texture and a high double-bounce content in the backscattered signal. In a future version of this algorithm a context-sensitive post-processing step will be used to remove anomalous classifications such as these.

IV. Results

The classifier was developed on the basis of SAR data for the training areas shown in Fig. 2. The classification results for pixels in the training areas are given in Table II, and the results for independent test areas are given in Table III. For both training and test areas, the classification accuracy exceeds 98% for three of the four classes, and for the fourth (short vegetation) the classification accuracy is better than 90%.

Note that classification accuracies are not given for the urban class. This has been done for two reasons: 1) since there is only one urban area, testing with the training area is unfair and misleading; and 2) since the urban area is not uniformly filled with urban features, but also contains trees, short vegetation, and surfaces, the classification accuracy calculated over the rectangular urban training stand will be inaccurate. The other three classes have accurate and uniform testing areas and so classification accuracies can be evaluated accurately. The urban class has been optimized so that it appears wherever buildings are known to occur, and does not appear within forested areas.

The classified image, shown in Fig. 5, contains a certain amount of "speckle," which presumably is a result of misclassification. These areas may also be correctly classified areas that are just areas of sparse vegetation surrounded by denser areas. In either case, one may want to apply an "aggregator" to the classified image. In comparing this image to a map produced through air photos, a certain amount of aggregating has already been performed on that data. In order to perform a fair comparison, the SAR classifier should apply a similar aggregation step. The aggregation algorithm used here is very simple: examine a 3 × 3 pixel region surrounding the pixel of interest and if over 70% of these pixels are a particular class, then the center pixel is assigned that class. Application of this aggregator improves the classification accuracy somewhat, but the image has dramatically less "speckle" (Fig. 6).

To allow a visual comparison of classification accuracy, a classification map from 15 years ago [14] is shown in Fig. 7. This map was manually interpreted from air photos. We have reclassified it so that only the four classes that our classifier uses are visible. Note that the airport was classed as an airport (land use) and that we have colored it as short vegetation since that is the majority of the land cover there. The city of Pellston is also a solid polygon because it is a land use rather than land cover map. The remainder of the map shows remarkable similarity to our classified image, except for the few new clear cuts.

The classification algorithm was also applied to a completely different site, Raco, imaged three months earlier, April 1. There are no large urban areas at this site, but

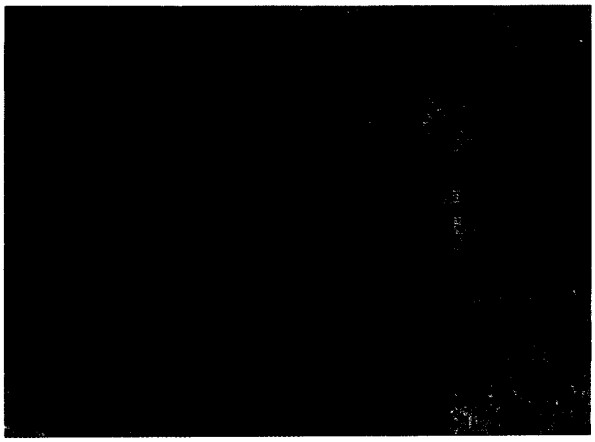

Fig. 6. Fully classified Pellston test site with aggregation. Urban is in white, tall vegetation is green, short vegetation is light brown, bare is blue.

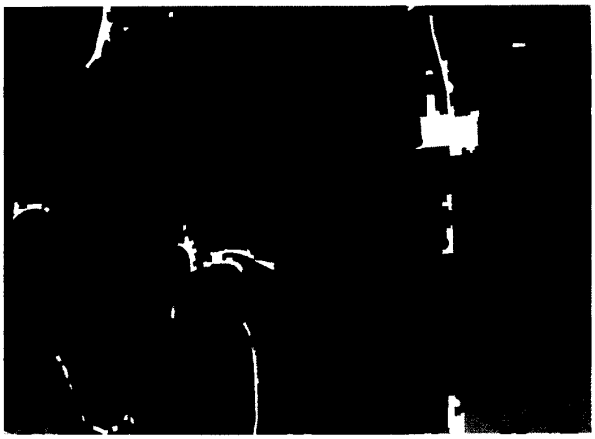

Fig. 7. Manually classified Pellston test site. Abstracted from Michigan DNR MIRIS data [14]. Urban is in white, tell vegetation is green, short vegetation is light brown, bare is blue.

TABLE II
Classification Accuracy, No Aggregation, Pellston Site, Training Areas, July

	True Class		
Classified As	Tall Veg	Short Veg	Bare
Tall Veg	98.32	0.00	0.00
Short Veg	1.46	94.74	0.87
Bare	0.00	5.26	99.07

TABLE III
Classification Accuracy, No Aggregation, Pellston Site, Testing Areas, July

	True Class		
Classified As	Tall Veg	Short Veg	Bare
Tall Veg	98.04	2.84	0.01
Short Veg	1.96	90.77	0.18
Bare	0.00	5.54	99.80

TABLE IV
CLASSIFICATION ACCURACY, NO AGGREGATION, RACO SITE, APRIL

	True Class		
Classified As	Tall Veg	Short Veg	Bare
Tall Veg	100.0	0.0	0.0
Short Veg	0.0	99.12	2.06
Bare	0.0	0.88	97.94

there are scattered buildings that are expected to be visible. Most of the area is a national forest and is largely pine trees. There are also many clearcuts visible with rough ground and many random logs strewn about. These are generally classified as short vegetation due to the small amount of biomass still present, but without vertical trunks. There is a large abandoned airport that provides the only smooth surface via its runways. When applied to this new image, the classification was equally successful, as seen in Table IV.

V. CONCLUSIONS

A polarimetric SAR image classifier has been designed and implemented that provides very good classification accuracies for the four classes: urban, tall vegetation, short vegetation, and bare surfaces. This classifier was developed with expert knowledge, with each class having its own classification rule, and proceeding in a sequential fashion. The classification rules are easy to understand and implement. Modification of the algorithm for special circumstances is therefore quite simple. The classifier uses rules that are as universal as possible, based on physical principles that are true for all incidence angles.

The aggregator is also a very simple context-sensitive addendum to the per-pixel classifier. The meaning behind its threshold is also quite clear: when over a certain percentage of one class, then it is all that class. This algorithm is also easily modified for special circumstances.

Future improvements to this algorithm may include a better way to distinguish urban pixels, and possibly a context-sensitive aggregator made specially for urban areas: so that a city park is classed urban rather than vegetation. Obviously, this kind of classification is user-driven: some investigators may want to know that there is a park in the city. Level-2 classifiers for each of the classes from this level-1 classifier are in the final stages of development.

REFERENCES

[1] F. T. Ulaby and C. Elachi, Eds., *Radar Polarimetry for Geoscience Applications*. Dedham, MA: Artech, 1990.
[2] D. N. Held *et al.*, "The NASA/JPL multifrequency, multipolarization airborne SAR system," in *Proc. IGARSS'88 Symp.*, Edinburgh, Scotland, 1988, pp. 317-322.
[3] J. J. Van Zyl and C. F. Burnette, "Bayesian classification of polarimetric SAR images using adaptive a priori probabilities," *Int. J. Remote Sensing*, vol. 13, p. 835, 1992.
[4] E. Rignot and R. Chellappa, "Segmentation of polarimetric synthetic aperture radar data," *IEEE Trans. Image Proc.*, vol. 1, p. 281, 1992.
[5] F.-Y. Wong and E. C. Posner, "A new clustering algorithm applicable to multispectral and polarimetric SAR images," *IEEE Trans. Geosci. Remote Sensing*, vol. 31, p. 634, 1993.
[6] R. O. Duda and P. E. Hart, *Pattern Classification and Scene Analysis*. New York, Wiley, 1973.
[7] M. Moghaddam and A. Freeman, "Modifications to the three-component classification algorithm for SAR data," presented at Electromagn. Res. Symposium (PIERS'93), July, 1993, Jet Propulsion Laboratory, California Institute of Technology.
[8] J. R. Kendra, F. T. Ulaby, and S. Wu, "A millimeter-wave technique for measuring ice thickness on the space shuttle's external tank," *Int. J. Infrared Millimeter Waves*, vol. 12, pp. 1349-1377, Dec. 1991.
[9] K. Sarabandi, "Derivation of phase statistics of distributed targets from the Mueller matrix," *Radio Sci.*, vol. 27, no. 5, p. 553, 1992.
[10] F. T. Ulaby, K. Sarabandi, and A. Nashashibi, "Statistical properties of the Mueller matrix of distributed targets," Special Issue IEE Proc. F, vol. 139, pp. 136-146, Apr. 1992.
[11] F. T. Ulaby, F. Kouyate, B. Brisco, T. H. Lee Williams, "Textural information in SAR images," *IEEE Trans. Geosci. Remote Sensing*, vol. GE-24, p. 235, Mar. 1986.
[12] T. M. Lillesand and R. W. Kiefer, *Remote Sensing and Image Interpretation*. New York: Wiley, 1987, ch. 10.
[13] A. Rosenfeld and A. C. Kak, *Digital Picture Processing*. New York: Academic, 1982, 2nd ed., ch. 5.
[14] Michigan State Dept. of Natural Resources, *Michigan Resource Information System (MIRIS)*, 1979.

Leland E. Pierce (S'85-M'85-M'89), for a photograph and biography please see page 984 of this issue.

Fawwaz T. Ulaby, for a photograph and biography please see page 985 of this issue.

Kamal Sarabandi (S'87-M'90-SM'93), for a photograph and biography please see page 984 of this issue.

M. Craig Dobson (M'80-SM'91), for a photograph and biography please see page 984 of this issue.